International Journal of Multiphase Flow 35 (2009) 760–772

Contents lists available at ScienceDirect

International Journal of Multiphase Flow

journal homepage: www.elsevier.com/locate/ijmulflow

On two-phase flow patterns and transition criteria in aqueous methanol and CO_2 mixtures in adiabatic, rectangular microchannels

C. Weinmueller, N. Hotz, A. Mueller, D. Poulikakos *

Laboratory of Thermodynamics in Emerging Technologies, Institute of Energy Technology, Department of Mechanical and Process Engineering, ETH Zürich, 8092 Zürich, Switzerland

ARTICLE INFO

Article history:
Received 23 January 2009
Received in revised form 26 March 2009
Accepted 29 March 2009
Available online 7 April 2009

Keywords:
Microchannel
Flow regime map
Two-phase flow
Phase transition
Micro fuel cells

ABSTRACT

This paper presents flow map investigations of adiabatic two-phase flow in square cross-sectioned, 200 μm deep microchannels fabricated in silicon, employing laser induced fluorescence microscopy. The influence of surface tension and nozzle geometry on the flow pattern transition was investigated using two nozzle widths (orifices of 30 μm and 50 μm, respectively) and methanol–water solutions with CO_2 as the gas phase. It was found and quantified that smaller nozzle geometries and smaller liquid surface tension promote the propagation of capillary gas bubbles at lower superficial gas and liquid velocities. Within the measurement domain of superficial gas (0.01–0.625 m/s) and liquid (0.0005–0.5000 m/s) velocities, we observed dispersed bubbly, regularly ordered bubbly, wedging, slug and annular flows, thus extending the experimental knowledge base to smaller superficial liquid velocities by almost two orders of magnitude. With the help of the flow maps presented herein, we were able to characterize the observed regularly ordered bubbly flow as the transition regime between dispersed bubbly and wedging flow. The results of the present investigation are of direct relevance to the operation of small-scale direct methanol fuel cells.

1. Introduction

Multiphase flow has been an ongoing subject of research activities ranging from large scale to, nowadays, microscale flow applications. The classical occurrence of two-phase flow includes the wide field of energy and process engineering with large-scale applications such as heat exchangers (Kattan et al., 1998; Kew and Cornwell, 1997; Thonon et al., 1995; Webb, 2004), chemical and biological reactors (Darmana et al., 2005; Dudukovic et al., 1999; Millies and Mewes, 1999; Vanhouten et al., 1994). Since the miniaturization trend of the electronics industry and decentralized energy conversion applications has initiated a host of innovative ideas in microfluidic applications such as Lab-on-Chip (Romera-Guereca et al., 2008), micro-chip cooling (Amon et al., 2001; Escher et al., 2009; Rosengarten et al., 2006; Senn and Poulikakos, 2004) or micro fuel cells (Choban et al., 2004; Hotz et al., 2006a,b; Senn and Poulikakos, 2005), a good understanding of the expected two-phase flow in the microchannels involved is necessary to design efficient devices. The many applications and technical occurrences (Gunther and Jensen, 2006; Joanicot and Ajdari, 2005; Kobayashi et al., 2004) combined with the complexity of the microscale physical phenomena involved, result in a challenging research task, even though large scale two-phase flow in channels has been reasonably well understood (Baker, 1954; Barnea and Taitel, 1993; Lockhart and Martinelli, 1949; Mandhane et al., 1974; Taitel and Dukler, 1976).

Whereas macroscopic two-phase flow is strongly influenced by the interaction of gravitational, inertia (shear) and surface tension forces, microscopic or capillary two-phase flow deviates from this description due to the diminishing influence of the gravitational force and a shift in the importance of the other mentioned forces. Kreutzer et al. (2005) suggested a classification of capillary/microscopic two-phase flow dependent on a critical Bond number derived analytically by Bretherton (1961):

$$Bo = \frac{\rho g d^2}{\sigma} < 3.368 \tag{1}$$

This criterion is derived for long bubbles moving upwards in a vertical, circular tube at low Reynolds numbers driven by buoyancy. At low Bond and Capillary numbers ($Ca = \eta u/\sigma$) the bubble motion is described by the lubrication theory. However, below a threshold (critical) value of the Bond number the bubble movement is terminated.

Despite the approximate nature of this classification in that it does not take dewetting phenomena, viscosity, or different channel cross-sections into account, it will be used in this paper, because it provides a simple means of classifying capillary/microscopic two-phase flows. The undisputable advantage of the critical Bond Number in defining the importance of microfluidic two-phase

* Corresponding author. Tel.: +41 44 632 2435; fax: +41 44 632 1176.
E-mail address: dimos.poulikakos@ethz.ch (D. Poulikakos).

0301-9322/$ - see front matter © 2009 Elsevier Ltd. All rights reserved.
doi:10.1016/j.ijmultiphaseflow.2009.03.010

Table 1
Parameter sets.

Parameter set	Channel geometry (μm)	Nozzle width (μm)	Liquid fluid
Set 1	200	50	H_2O
Set 2	200	50	1 M MeOH
Set 3	200	50	MeOH
Set 4	200	30	1 M MeOH

phenomena is the incorporation of the surface tension, a clear improvement over classifications based on channel dimensions only.

Questions whether correlations obtained from macroscopic experiments still hold, whether the same set of forces play a role and to what extend, have to be further addressed. To this end, many recent publications (Coleman and Garimella, 1999; Cubaud and Ho, 2004; Hassan et al., 2005; Kreutzer et al., 2005; Triplett et al., 1999; Waelchli and von Rohr, 2006; Zhao and Bi, 2001) indicate advances in this field, but the influence of surface tension and nozzle geometry on the phase transition was not taken into consideration. This study focuses on the influence of surface tension, by examining three different liquid mixtures of a methanol–water solution, with carbon dioxide as the gas phase, see Table 1. In addition, a set of nozzle geometries, see Table 1, have been studied in order to deduce the influence on flow regime transitions. The choice of the working fluids is based also due to its relevance to small-scale direct methanol fuel cells.

A reference case (parameter set 01, see Table 1) has been established in order to objectively compare with similar parameters (fluid properties, channel geometry and fabrication techniques) in the literature before the influences of surface tension and nozzle geometry can be discussed. In addition, the future need (Gunther and Jensen, 2006; Hassan et al., 2005) for flow maps at lower liquid flow rates has been addressed by this study. The existing knowledge of two-phase flow transitions has been extended by almost two orders of magnitude in square microchannel flow maps of 200 μm edge length.

2. Experimental procedure

2.1. Microfabrication

A standard microfabrication/MEMS technique (Madou, 2002) based on photolithography was applied to manufacture micro-sized channel networks, see the fabrication steps in Fig. 1. In a first step a 500 ± 25 μm thick, p-doped, double side polished, 4″ silicon wafer with a resistivity of up to 30 Ω cm was coated with at 10 μm thick layer of a negative photoresist (AZ® 4562, MicroChem). In the subsequent photolithographic process step (MA6, Süss Micro Tec), the mask polarity of the deployed high resolution quartz mask (ML&C) patterns the photoresist during the UV exposure. A dry etching procedure was performed using an inductive coupled plasma system (ICP, Surface Technology Systems) resulting in a rectangular shaped channel cross-section with a depth and width of 200 μm. The surface roughness of the channel walls is defined by the cycle length of the involved "Bosch process" and the mask resolution, and does not exceed 1 μm. By the iteration of the above mentioned steps at the backside of the silicon wafer, fluid inlets, outlets and pressure ports are incorporated. To allow for optical access, a 100 mm in diameter and 700 ± 50 μm thick borosilicate glass wafer was anodically bonded onto the silicon wafer by a substrate bonder (SB6, Süss MicroTec) at 450 °C and a voltage of 1000 V. After dicing the wafer into predefined microchannel chips, PEEK (Upchurch Scientific®) fluid connectors were sealed to the inlet, outlet and pressure tubes by epoxy.

The microfluidic network on the chip has been designed in accordance to representative microreactors, for the applicability of micro fuel cell designs (Lu et al., 2004) and in comparison to existing microfluidic investigations (Cubaud and Ho, 2004; Waelchli and von Rohr, 2006). A distinct difference from the design of Cubaud and Ho (2004) is that the rounding off of the serpentine bends herein was deliberately realized, to reduce inertia effects resulting from the momentum exchange with the wall, especially at sharp turns, diminishing the influence onto the two-phase flow. Micro-PIV investigations (Fries et al., 2008) mention the possibly important influence of momentum exchange in the bends to fluid mixing in the liquid plugs in the wake of a segmented gas–liquid flow, but only corroborate the unaffected flow pattern.

The mixing section of the microchannel is of crucial importance to the formation of the two-phase flow (Cubaud et al., 2005). The liquid stream is divided into two equal pathways (in length and volumetric flow resistance) by a T-junction. At the mixing zone, the two liquid flows enclose the introduced gas flow coming at a right angle, see (Cubaud et al., 2005; Dollet et al., 2008; Ganan-Calvo and Gordillo, 2001). The so-described, layered flow passes through an orifice of 200 μm depth and 50 μm widths, accelerating the flow. The abrupt expansion after the orifice to the channel dimensions of 200 × 200 μm^2 leads to the formation of a bubble, as detailed in (Dollet et al., 2008; Ganan-Calvo and Gordillo, 2001).

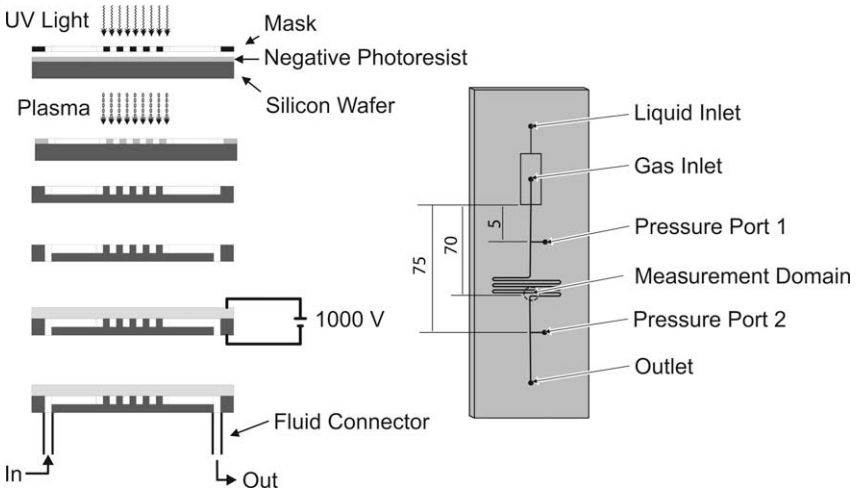

Fig. 1. Process flow for the fabrication of the microchannel chip illustrating photolithography, photoresist development, dry etching by ICP, backside process, anodic bonding and the attachment of the fluid connector – and a top view of a typical microchannel chip.

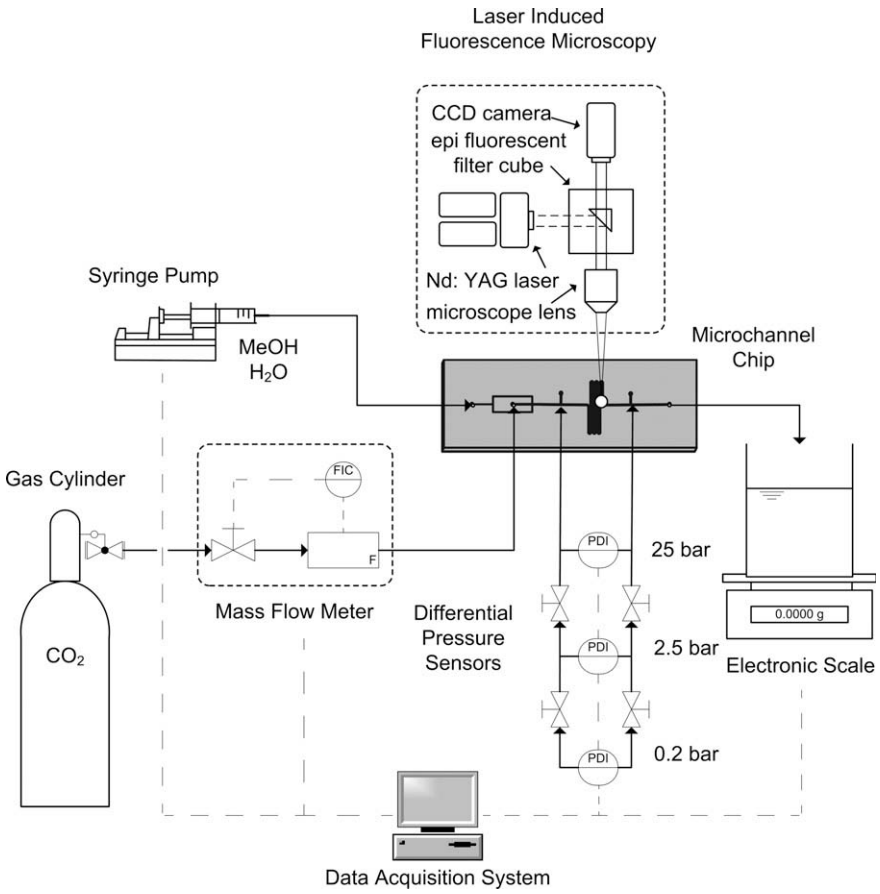

Fig. 2. Schematic diagram of the experimental apparatus.

2.2. Experimental setup

The experiments were performed under standard laboratory conditions, at 22 °C and 100 kPa ambient, in the experimental apparatus shown in Fig. 2. A syringe pump (Harvard Apparatus, PHD4400 programmable) delivers the desired fluid flow $\dot{V}_l$ of the aqueous methanol solution ranging from 0.0012 to 1.200 ml/min. Several different methanol concentrations have been experimentally investigated. The corresponding parameter sets are listed in Table 1, and the respective fluid properties in Table 2.

The volumetric flow rate $\dot{V}_g$ of the CO_2 gas stored in a pressurized gas cylinder (PanGas, purity $\geqslant$ 99.9 vol%) is adjusted by a mass flow controller (Bronkhorst, EL-FLOW®) from 0.02 to 1.5 ml/min. Both fluid flows are transported through PEEK (Upchurch Scientific®) capillaries and injected through the corresponding inlets into the microchannel chip. At the mixing zone, a nozzle working by the principle of the capillary flow focusing technique (Cubaud et al., 2005; Dollet et al., 2008; Ganan-Calvo and Gordillo, 2001), forms the two-phase flow pattern. In the subsequent section of the microchannel, the resulted flow pattern was investigated over a serpentine-structured channel length. As mentioned earlier, the serpentine bends are designed with smooth, rounded bends in order to reduce the influence of momentum exchange effects with wall.

After 5 mm ($25 \times d_{hyd}$) from the nozzle, well outside of the hydraulic entrance length, the first pressure port is incorporated, with the second one being located at the end of the area of investigation. Precisely 70 mm of channel length lie between these two ports. Three differential pressure sensors (Huba Control 692; 0.2 bar, 2.5 bar, 25 bar) have been employed for recording the pressure drop between the two pressure ports depending on the flow rates. After passing through the area of observation, 70 mm downstream from the nozzle, the two-phase flow exits the microchannel chip by a PEEK tube and is collected in a glass beaker open to the ambient positioned on an electronic scale (Mettler Toledo XS204 DeltaRange®) for cross-checking of the liquid flow rate.

The data collected from the syringe pump, the mass flow meter and the differential pressure sensors are recorded by a data acquisition system (Labview 7.0), however, the controlling of the mass flow meter is performed by a Bronkhorst specific program, FLOWView®.

Table 2
Fluid properties.

Fluid mixture	Density (kg/m^3)	Viscosity (mPa s)	Surface tension (mN/m)
H_2O	997.1	1.0016	72.75
1 M MeOH	980.2	1.0982	66.10
MeOH	786.9	0.5440	22.95
CO_2	1.811	0.0150	–

2.3. Fluorescence microscopy

There exist several, non-intrusive methods for characterizing flow patterns in microchannels, such as Brightfield microscopy, fluorescence microscopy, transient magnetic resonance imaging. In contrast to the commonly used Brightfield microscopy, the herein presented experiments were conducted utilizing a fluorescence microscopy technique (LaVision Flow Master MITAS), see Fig. 2.

The liquid mixture was doped with 0.01 wt% Rhodamine 610 Chloride (Exciton), a fluorine dye also known under Rhodamine

B, to achieve a distinguishable contrast between the fluorescent liquid and the non-luminating gas phase. This concentration is expected to reduce the surface tension of the liquid mixture by around 5%. A double cavity Nd:YAG laser (New Wave, SoloII-15, 532 nm) with a pulse length of 10 ns was applied as a light source exciting the fluorescent dye in the liquid. Rhodamine 610 Chloride re-emits light with a phase shift at a wavelength of around 594 nm depending on the present solvent. An epi-fluorescent filter cube (dichromatic prism) prevents the laser pulse from trespassing; only the re-emitted light reaches the synchronized CCD-camera chip (LaVision Imager ProX 4 M) with a set exposure time of 500 ns yielding distinct two-phase flow images as presented in Fig. 3.

3. Flow pattern

3.1. Classical categorization

The injection of two immiscible fluids of different densities into an adiabatic microchannel leads, after a certain entrance length, to a distinct flow regime depending on fluid properties, channel geometry and volume flow rates of the two fluids. For the case of a single pair of gas–liquid mixture in a given channel, a flow regime map can be constructed based on the gas and liquid volume flow rates.

Different volume flow rates will yield a series of distinguishable regimes. Attempting to find in the plethora of published regimes a

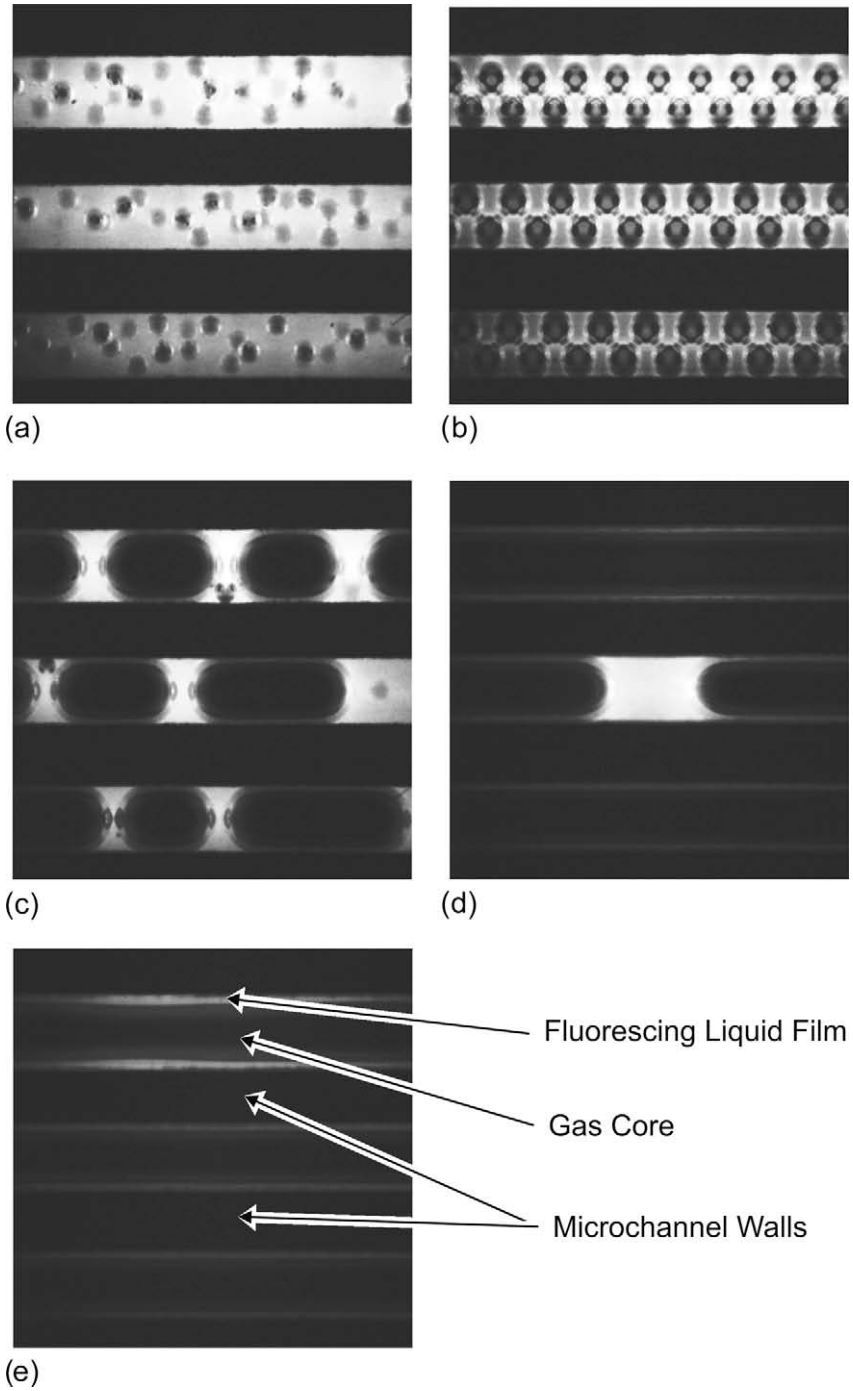

Fig. 3. Micro-PIV images from: (a) bubbly, (b) regularly ordered bubbly flow, (c) wedging, (d) slug, and (e) annular flow.

Table 3
Flow pattern.

Major flow regime	Flow pattern
Dispersed	Dispersed bubbly
	Regularly ordered bubbly
Intermittent (Taylor)	Wedging (elongated bubbly, plug)
	Slug flow
Annular	Smooth annular
	Wavy annular
Stratified	Smooth stratified
	Wavy stratified

common denominator for representative regimes and their descriptions, this paper relies on a combination of classifications from Kreutzer et al. (2005), Coleman and Garimella (1999) and Cubaud and Ho (2004) with a minor modification, see Table 3. This has been chosen as a base for comparison because of the similarity in channel geometry, which includes a similar order of magnitude of a rectangular cross-section as well as the aspect ratio.

As reported elsewhere (Coleman and Garimella, 1999), a significant difference of flow regimes can be observed between a channel of circular and rectangular cross-sections. This additional complexity and therefore deviation potential for flow regimes is amplified by the effect of aspect ratios. Since the first investigations of two-phase flow in a micro-spaced rectangular cross-sectioned channel have been performed in narrow widths or slit configurations, the applicability of those derived flow maps for a rectangular cross-section channel is questionable.

The flow regime modification is the existence of a regularly ordered bubbly flow pattern in addition to the dispersed flow regime. Under a different context, bubble formation by hydrodynamic focusing for application of e.g. single microbatch reactors (Joanicot and Ajdari, 2005), the so-called regularly ordered bubbly flow is referred to as bubble-liquid suspension (Gordillo et al., 2004), monodispersed array of bubbles (Cubaud et al., 2005) or lattices of bubbles (Ganan-Calvo and Gordillo, 2001), but is has not been incorporated into any flow map categorization to the best of the authors' knowledge. Since the described bubble arrangement (see next section) consists of perfectly spherical bubbles, see Fig. 3(b), of the same diameter, the term *foam*, describing and referring to polyhedral-shaped, deformed gas volumes, is inappropriate to use.

The typical working fluids for investigating two-phase flow in the literature are water–air or water–nitrogen mixtures, hence the regularly ordered bubbles have not been observed under the context of flow map investigations. A discussion and description of the flow regimes will be presented in the following section.

3.2. Observed flow regime descriptions

3.2.1. Dispersed flow regime

As mentioned earlier and illustrated in Table 3 the dispersed flow regime is subdivided into two parts. Starting at a low gas flow rate a dispersed bubbly flow will occur, see Fig. 3(a). The gas phase can be described as discrete spheres with diameters smaller than the channel height distributed rather uniformly in the continuous liquid phase. An increase of the gas flow rate yields an increase of the bubble size until the diameter starts to surpass the channel height. From that moment on, since the bubble is constrained by the channel cross-section, the flow regime is referred to as intermittent.

However, under certain conditions an increase in the gas flow rate will not cause an increase of the bubble size, but an increase of bubble quantity to such a level, that the single gas spheres are starting to densely pack inside the constraints given by the channel geometry, see Fig. 3(b). Coalescence of bubbles (Ostwald Ripening), as reported by some authors, has not been observed at distinct volume flow rates. The criteria for coalescence are not discussed in this paper. This paper will refer to such a flow pattern as regularly ordered bubbly flow.

3.2.2. Intermittent flow regime

The intermittent flow regime is known under a bounty of different expressions, elongated bubbly, wedging, slug, plug or segmented flow, but often attributed to Taylor and his work (Taylor, 1960). The characteristic of this flow pattern is a gas bubble, which has a lager dimension than the cross-section of the channel. Due to the dominance of the surface tension, the bubble expands along the channel axis rather than collapsing or disintegrating into smaller spherical bubbles.

Two distinguishable flow patterns can be detected within the range of the intermittent flow regime, the wedging and the slug flow, see Fig. 3(c) and (d), respectively. Even though the geometric appearance of the two flow patterns is similar and can be described by an axisymmetric gas core surrounded by a thin liquid film and regularly segmented by liquid plugs, forming an elongated gas bubble, the wedging flow regime exhibits under certain circumstances (Cubaud and Ho, 2004) a de-wetting and dry-out along the center of the adjacent channel walls.

In contrast, the slug flow pattern is characterized by a much larger and, therefore, stronger elongated gas bubble, which does not exhibit any dry-out zones. The gas core will be lubricated at all times by the fast passing liquid slugs.

As described by Cubaud and Ho (2004), the wedging flow regime can be divided into two different wetting regimes dependent on the bubble velocity with a transition regime in between. If the bubble velocity is below the dewetting velocity, the liquid film between the elongated gas bubble and the channel walls will dry out. If the bubble velocity is above a critical velocity, the film will not be disrupted and the bubble will be surrounded by a liquid film.

3.2.3. Annular flow

At low liquid velocities, the liquid plugs spanning the channel cross-section disappear with increasing gas velocities forming rings or waves and eventually smoothing out; a continuous, axisymmetric gas core establishes itself, see Fig. 3(e). The liquid volume flow is transported merely in the thin liquid film covering the channel walls.

3.2.4. Stratified flow

The stratified flow has not been observed herein, but is shortly elaborated upon for the sake of completeness and its presence in some of the flow maps to be discussed in the following. The stratified flow regime exhibits a complete separation of the liquid and the gas phase. In large scale two-phase flow, this separation is induced by the buoyancy force, whereas for microscopic channel dimensions the wettability of the surface in combination with the surface tension usually inhibits a stratified flow.

3.3. Results

3.3.1. Flow maps of parameter sets 1–4

The results of our experiments are discussed in this section, followed by a thorough comparison with previously published investigations. In Fig. 4(a)–(d) the results of four parameter sets are shown. Parameter set 1 has been defined as a reference case for comparison with relevant literature fluid-gas mixtures (Coleman and Garimella, 1999; Cubaud and Ho, 2004; Triplett et al., 1999; Zhao and Bi, 2001). In the parameter sets 1–3, only the concentration of the methanol–water solution is altered, as seen in Table 2, starting with destilled water for parameter set 1, followed by a 1 M methanol solution for the parameter set 2 and a pure MeOH

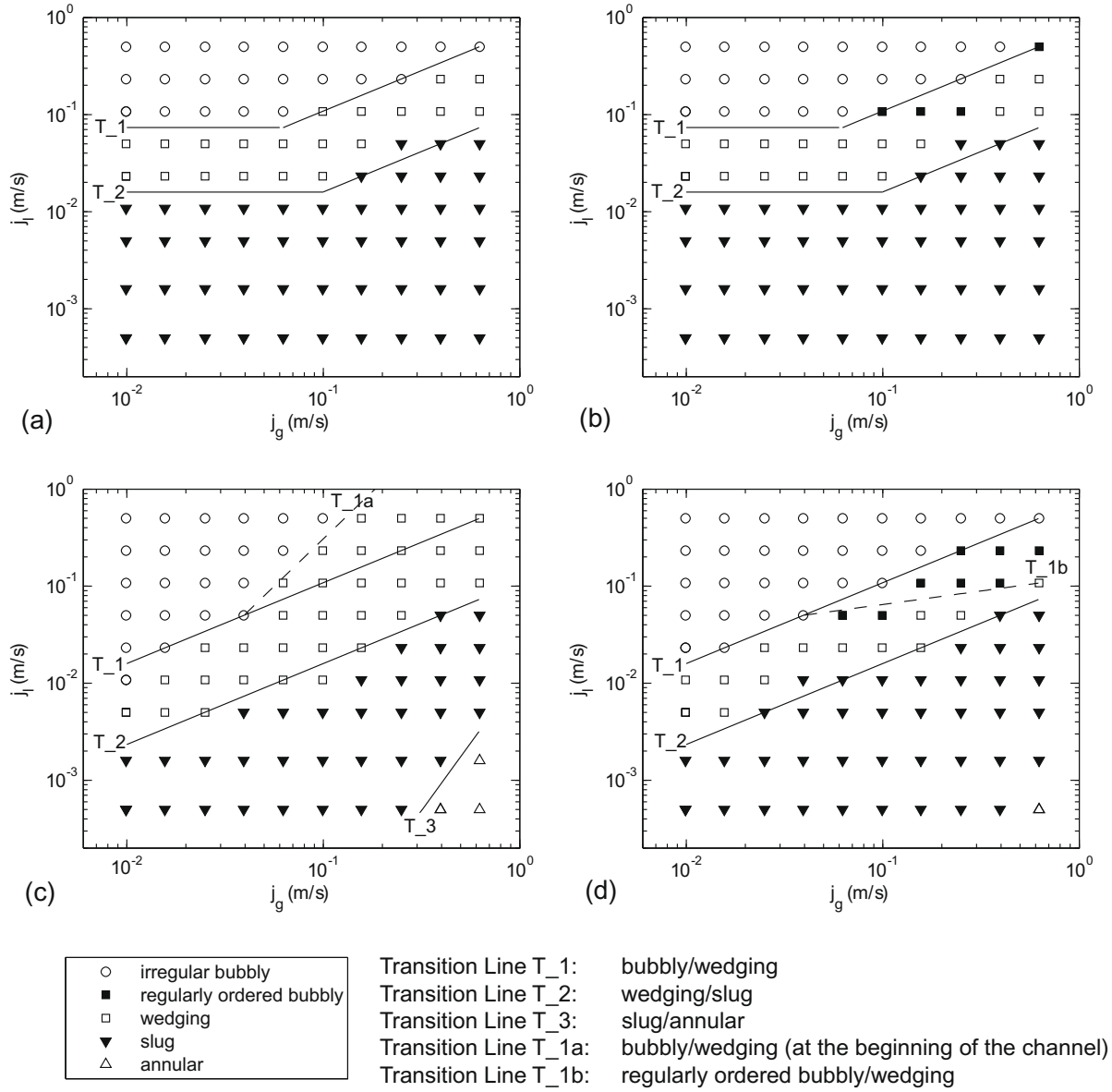

Fig. 4. Flow regime maps for squared microchannels: (a) parameter set 1: nozzle 50 μm, pure H_2O; (b) parameter set 2: nozzle 50 μm, 1 M MeOH solution; (c) parameter set 3: nozzle 50 μm, pure MeOH; and (d) parameter set 4: nozzle 30 μm, 1 M MeOH solution.

solution for parameter set 3. In parameter set 4 the liquid has the same concentration as for parameter set 2, but the geometry of the nozzle is altered to a smaller width of 30 μm in order to identify possible influences of the nozzle geometry.

The experiments were conducted by setting a certain liquid flow rate at the syringe pump and stepwise increasing the gas flow rate. The gas flow rate was allowed to reach steady state conditions, but at least 300 s were allowed to pass before the flow pattern was recorded and identified at a location 70 mm downstream from the nozzle exit, well after the hydraulic entrance length and in between the pressure ports.

The recorded flow patterns are displayed in a graph with the superficial gas velocity j_g constituting the abscissa and the superficial liquid velocity j_l constituting the ordinate, see Fig. 4(a)–(d). The superficial gas velocity j_g is defined as the gas volume flow rate V_g divided by the total cross-sectional area A of the channel, analogously to the superficial liquid velocity:

$$j_l = \frac{\dot{V}_l}{A} \tag{2}$$

An interesting observation can be drawn from all four parameter sets 1–4 concerning the transition lines between the bubbly, wedging and slug flow regimes. At superficial gas velocities $j_g \geqslant 0.08$ m/s (the rms of $j_g \geqslant 0.06$–1.0 m/s) in the parameter sets the transition lines T_1 and T_2 are parallel with identical slopes and positions on the flow map allowing the assumption that the change of liquid properties within the parameters studied in this paper and the slight alteration of the nozzle orifice has no significance on the main trend of the two transition lines at the bubbly/wedging flow transition and the wedging/slug flow transition, referred to subsequently as transition lines T_1 and T_2 respectively. The transition line separating the bubbly from the wedging flow regime can be mathematically expressed as follows:

$$\text{Transition line T\_1}: \quad j_l = 0.7397 \cdot j_g^{0.8333} \tag{3}$$

The parallel positioned transition line of the wedging to slug flow regime (T_2) yields a similar, exponential function as for transition line T_1, with the same exponent, but with a different offset:

$$\text{Transition line T\_2}: \quad j_l = 1.086 \cdot j_g^{0.8333} \tag{4}$$

In Fig. 4(a), below the critical value of $j_g = 0.08$ m/s (parameter sets 1 and 2 (only) at $j_g = 0.08$ m/s) the transition between bubbly to wedging flow (T_1) becomes independent of the gas flow rate. This transition only depends on the liquid volume flow rate. The transition is located at:

$$j_l = 0.0736 \cdot \mathrm{m/s} \tag{5}$$

In comparison to parameter set 3, the transition is further dominated by the ratio of the two liquid flow rates, because the methanol as a liquid with a considerably lower surface tension than water stabilizes smaller bubbles at the same nozzle geometry. This can be explained by the working principle of the flow focusing technique. The detachment of the gas core forming a bubble (or Taylor bubble) depends upon the interaction between inertia and surface tension. The lower the surface tension, the earlier the break off from the gas core occurs and the smaller the formed bubbles will be. This can also be facilitated by a smaller nozzle geometry, as seen in the results of parameter set 4, shown in Fig. 4(d). Summarizing, it can be said that two mentioned effects cause a stabilization of smaller bubbles below the critical value of $j_g = 0.08$ m/s; this is achieved either by reducing the nozzle geometry below 50 μm or by reducing the surface tension of the liquid.

An analogous argument holds for the transition from wedging to slug flow (T_2) with a transition line positioned at:

$$j_l = 0.0159 \cdot \mathrm{m/s} \tag{6}$$

The effect of a slightly reduced surface tension of the liquid by the 1 M methanol solution seen in parameter set 2, Fig. 4(b), does not show a marked influence on the transition lines of parameter set 1, Fig. 4(a). Interestingly however, the occurrence of the regularly ordered bubbly regime can be detected inside the perimeter of the wedging flow regime, between transition line T_1 and T_2. This indicates that the addition of a small amount of methanol stabilizes smaller bubbles due to an earlier break off of the gas core at the nozzle. At the same time, the surface tension is high enough to prevent coalescence of the individual gas bubbles, forming a regularly ordered bubbly regime. The regularly ordered bubbly regime is further detected in parameter set 4, see Fig. 4(d), which can be explained similarly as for the 1 M methanol solution.

For parameter sets 3 and 4, the appearance of a transition region above $j_g = 0.04$ m/s is of interest. In the case of parameter set 3, the mixing of methanol in the solution yields a phase transition in the microchannel from a bubbly to a wedging flow regime. The transition was complete within ca. 70 mm downstream from the nozzle and is characterized by the following transition line:

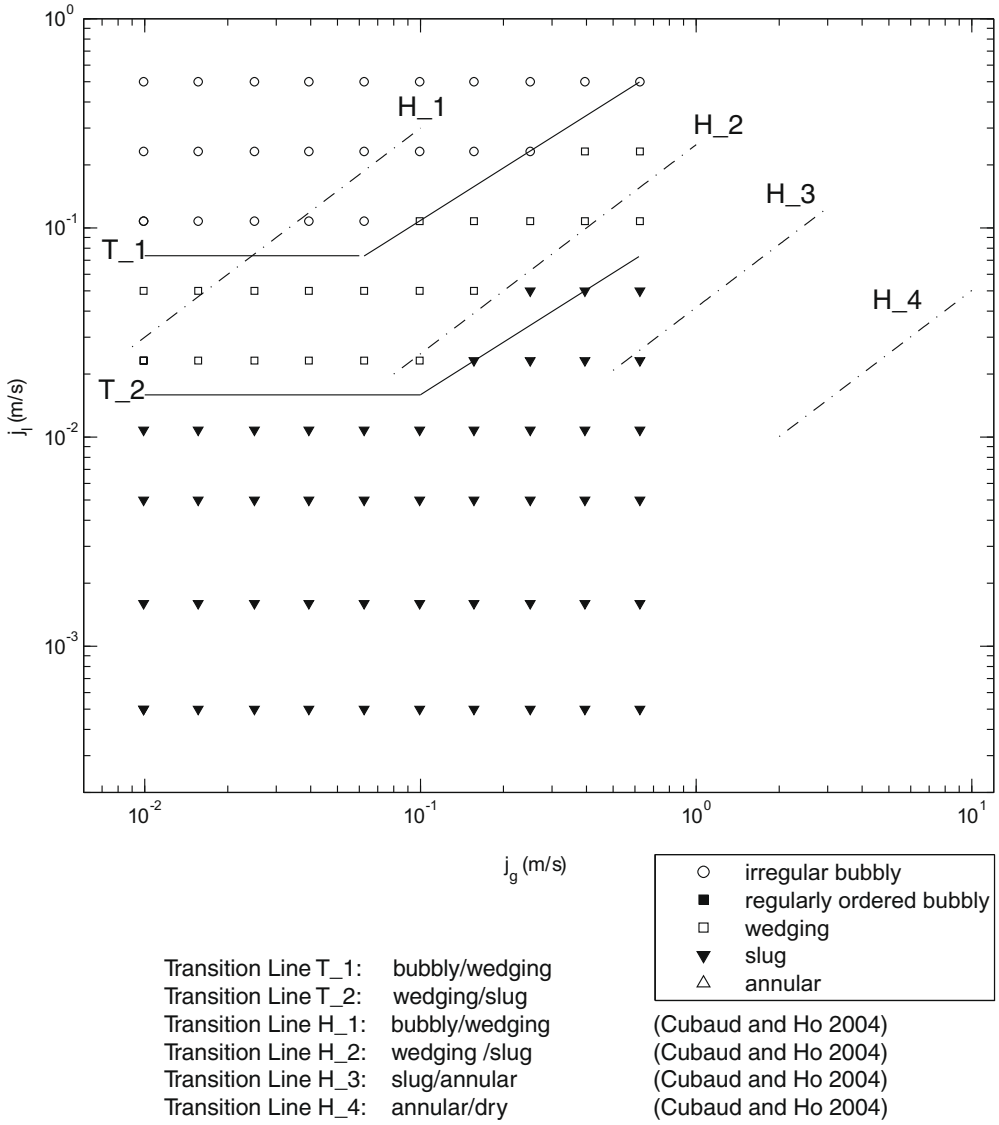

Fig. 5. Flow map comparison to Cubaud and Ho (2004).

Transition line T_1a $j_l = 27.388 \cdot j_g^{1.9503}$ (7)

For parameter set 4, a regularly ordered bubbly flow regime appears as a transition regime below T_1 bounded by

Transition line T_1b $j_l = 0.1228 \cdot j_g^{0.2778}$ (8)

The only occurrence of an annular flow regime has been detected in the parameter sets 3 and 4, see Fig. 4(c). A regression line for the transition between the slug and the annular regime based on three annular regime data points bears a high uncertainty, but is presented for sake of completeness:

Transition line T_3 $j_l = 0.012 \cdot j_g^{2.7824}$ (9)

3.4. Comparison to existing flow maps

In the following sections the most relevant, recent and influential micro two-phase flow investigations will be compared to our experimental data. The experiment with apparently the most similar realization has been presented by Cubaud and Ho (2004).

3.4.1. Flow map comparison to Cubaud and Ho (2004)

Cubaud and Ho (2004) investigated thoroughly two-phase flow in rectangular channels with a square cross-section of side widths of 200 μm and 500 μm. The microchannels were fabricated by deep reactive ion etching (DRIE) into silicon covered by an anodically bonded glass on top and bottom allowing optical access. The working fluids they used were de-ionized water and compressed air mixed by a flow-focusing nozzle. The nozzle proved to be an effective measure in producing bubbles in a large range of sizes. They observed downstream from the nozzle section bubbly, wedging, slug, annular and dry flow, presented in a classical two-phase flow map, see Fig. 5.

The transition lines of the flow map of Cubaud and Ho (2004), based only on the 200 μm channel, are drawn as a reference for comparison to our experimental data. In (Cubaud and Ho, 2004) the assumption was made that the flow map within the boundaries of their measurement domain is independent of the size of the channel cross-section. After an extrapolation of the transition lines into the regime of 500 μm channels, their findings yield the following, generalized functionality for the dependence of the superficial velocities:

$$j_g = \frac{\alpha}{1-\alpha} \cdot j_g \quad (10)$$

with $\alpha = 0.75$ for bubbly/wedging transition (T_1), $\alpha = 0.20$ for wedging/slug transition (T_2), $\alpha = 0.04$ for slug/annular transition (T_4), $\alpha = 0.005$ for annular/dry transition.

The comparison of the data of Cubaud and Ho (2004) obtained from the 200 μm cross-sectional microchannels to our experimental data, shows a good agreement of the phase transitions between bubbly/wedging flow (T_1) and wedging/slug flow (T_2), see Fig. 5. A deviation of the transition lines T_1 can be observed. However, after a closer examination of the regression of the transition line H_1 in Cubaud and Ho (2004), it can be noted that this transition line does not accurately capture the phase transition for the 200 μm cross-section microchannels alone. Several points of their data set of the bubbly flow do not fall within the proposed bubbly regime. If for the same set of their data points (200 μm values only) the phase transition of Cubaud and Ho (2004) is interpreted separately, the transition line slopes more gradually, practically superimposing with our result for T_1.

The plateaus of the transition lines T_1 and T_2 occurring in our study below the value of $j_g = 0.08$ m/s; have not been detected in Cubaud and Ho (2004). The reason is that our larger nozzle design, the orifice has the same depth as the channel following it, can stabilize larger elongated bubbles at smaller gas volume flow rates.

The phase transitions between slug/annular and annular/dry flow as depicted in Cubaud and Ho (2004) are not within our measurement region, therefore, a fair comparison cannot be conducted. If one assumes an exponential (linear in log scale) extrapolation of the transition line into our measurement domain, a deviation could be expected. A possible explanation can be deduced from our classification of the slug flow regime, which includes an annular-similar flow regime with a scarcely occurring slug passing down the channel.

Unlike the work of Cubaud and Ho (2004), the dry flow regime has not been observed for the 200 μm being in accordance with many other studies (Coleman and Garimella, 1999; Triplett et al., 1999).

Summarizing, the conclusions drawn from the comparison between our study and that of Cubaud and Ho (2004), it can be said that the channel size has an influence on the transition lines as well. The extrapolations of the findings of Cubaud and Ho (2004) from two different channel sizes are not showing the plateaus found in our study underpinning the conclusion that the phase transition of microscale two-phase flow is not only dependent on the channel geometry (Coleman and Garimella 1999), but also on the channel size (Triplett et al., 1999; Zhao and Bi, 2001). In general, it can be stated that the flow map of Cubaud and Ho (2004) corroborates well our phase transitions.

It should be also stated that we were able to measure two orders of magnitudes lower than Cubaud and Ho (2004), extending the so far known flow regime map for microscale two-phase flows, detecting a dominant slug flow regime below the critical value of $j_l = 0.0159$ m/s.

3.4.2. Flow map comparison to Triplett et al. (1999) and Zhao and Bi (2001)

Further comparison to often referred and cited papers is necessary in order to understand and extract the influential parameters on the transition lines. In the following, the work from Triplett et al. (1999) and Zhao and Bi (2001) is used as a further means toward this goal and is presented in comparison to our data in Fig. 6.

Triplett et al. (1999) observed in their Pyrex glass channels with circular and triangular cross-section with a hydraulic diameter of 1.1 mm and 1.45 mm, respectively, four distinguishable flow regimes: bubbly, slug, churn and annular-wavy. The orientation of the setup was horizontal and the fluids, de-ionized water and air, were mixed in a cross-like mixing chamber and co-currently passed through a 200 mm long tube of the above mentioned geometries.

Zhao and Bi (2001) tested three equilateral triangular channels fabricated of Lucite Plastic. In contrast to Triplett et al. (1999) and Cubaud and Ho (2004) a vertical upwards concurrent two-phase flow was established by water and air injection through a porous medium. The resulting flow regimes were: capillary-bubbly, slug, churn and annular flow.

A first obvious/apparent observation extracted from a direct comparison of our measurement data to the phase transition lines presented from Triplett et al. (1999) and Zhao and Bi (2001) is the difference of the measurement domains, see Fig. 6. To this end, besides the shifted area of observation (Triplett et al., 1999: $j_g = 0.02$–80 m/s and $j_l = 0.02$–8 m/s; Zhao and Bi, 2001: $j_g = 0.1$–100 m/s and $j_l = 0.08$–6 m/s), also the different channel geometries have to be borne in mind when drawing conclusions from the comparison.

It is most interesting that our entire measurement range lies within the expected slug flow regime based on the flow map of Triplett et al. (1999) of circular channel cross-sections and of the flow map of Zhao and Bi (2001) of triangular microchannels. Besides the explanation of the different channel geometries for the

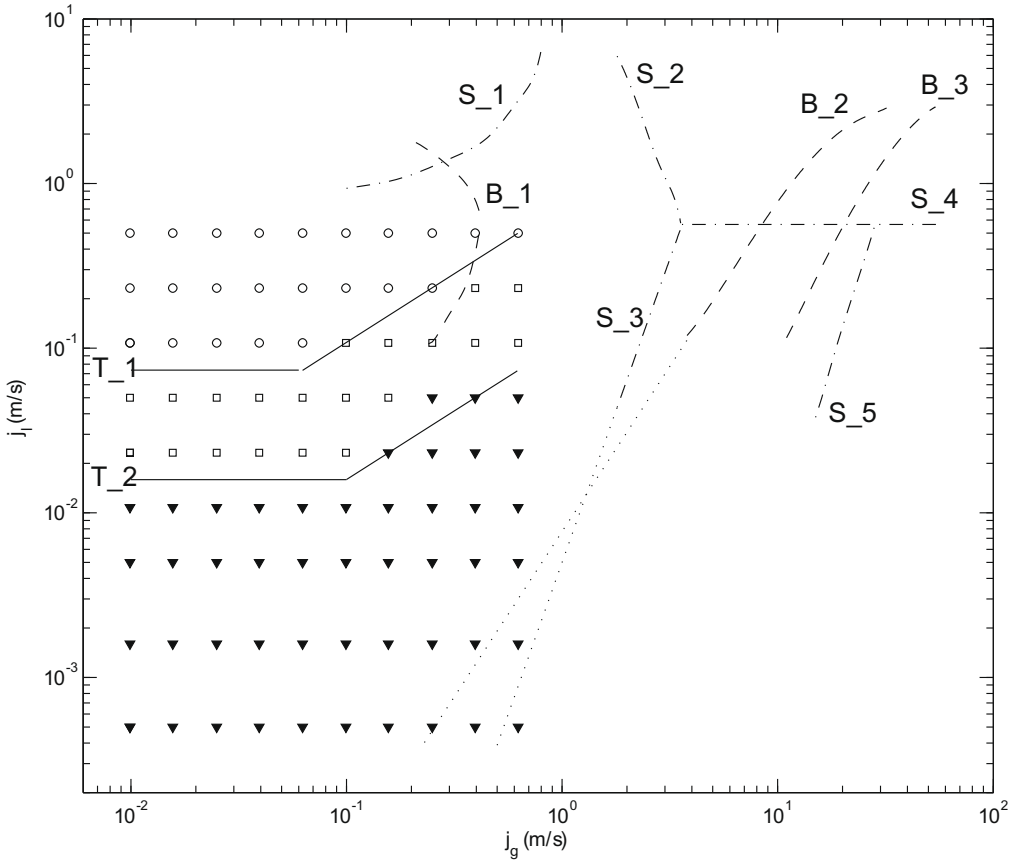

○	irregular bubbly
■	regularly ordered bubbly
□	wedging
▼	slug
△	annular

Transition Line T_1:	bubbly/wedging	
Transition Line T_2:	wedging/slug	
Transition Line S_1:	bubbly/slug	(Triplett et al. 1999)
Transition Line S_2:	slug/churn	(Triplett et al. 1999)
Transition Line S_3:	slug/slug-annular	(Triplett et al. 1999)
Transition Line S_4:	churn/annular	(Triplett et al. 1999)
Transition Line S_5:	slug-annular/annular	(Triplett et al. 1999)
Transition Line B_1:	bubbly/slug	(Zhao and Bi 2001)
Transition Line B_2:	slug/churn	(Zhao and Bi 2001)
Transition Line B_3:	churn/annular	(Zhao and Bi 2001)

Fig. 6. Flow map comparison to Zhao and Bi (2001) and Triplett et al. (1999).

deviation, special notice should be drawn to the nozzle. As proven elsewhere (Cubaud et al., 2005; Ganan-Calvo and Gordillo, 2001), the nozzle has a significant influence on stabilizing bubbles especially in microchannels ($Bo < 3.368$). Certain orifice geometries can facilitate a broad range of bubbles, sometimes referred to as capillary bubble flow (Zhao and Bi, 2001).

This explanation supports our finding of bubbly and wedging flow also at lower j_l than reported from Triplett et al. (1999). On the other hand, under the consideration of the aforementioned deviation factors, the bubbly regime detected from Zhao and Bi (2001) is in rather good agreement with our results. Nevertheless, the possibility of a coincidental superimposition of the phase regimes cannot be completely excluded.

Interestingly, the extrapolations of the lines of the phase transition between slug and ring-annular flow from the work of Triplett et al. (1999) and of Zhao and Bi (2001) are approximately superimposing the phase transition line for the methanol solution displayed in Fig. 4(c).

The comparison to Coleman and Garimella (1999) does not reveal any new information; our flow map lies completely in their plug/slug flow regime, an analogous discussion as for Zhao and Bi (2001) and for Triplett et al. (1999) applies.

3.4.3. Comparison to the Taitel–Dukler model

An influential paper presenting a physical model to describe the phase transition in macroscopic two-phase flow in a horizontal (and near horizontal) circular tube has been published by Taitel and Dukler (1976). The model is based on the equilibrium of the momentum balances of each single phase (gas and liquid separately) of a stratified two-phase flow with a power law friction factor assumption for the shear forces (Agrawal et al., 1973). A dimensionless representation of the momentum balances was expressed as a function of X, the Lockhart–Martinelli-Coefficient (Lockhart and Martinelli, 1949), and the dimensionless parameter Y representing the influence of the inclination. For the case of zero inclination, as studied and compared in this work, the Lockhart–Martinelli-Coefficient X only depends on the dimensionless equilibrium filling height $\tilde{h}_l = h_l/D$ of the liquid phase. Taitel and Dukler (1976) developed for each phase transition a criterion representing it by one specific dimensionless number.

The transition of the stratified to intermittent flow is based on the Kelvin–Helmholtz stability criterion for the growth of infinitesimal waves at a liquid/gas interface with a critical filling height of 50% of the inner diameter of the tube, which can be expressed in a dimensionless form as:

$$F^2\left[\frac{1}{C_2^2}\frac{\tilde{u}_g d\widetilde{A}_l/d\tilde{h}_l}{\widetilde{A}_g}\right] \geqslant 1 \tag{11}$$

where F is a modified Froude number:

$$F = \sqrt{\frac{\rho_g}{\rho_l - \rho_g}}\frac{j_g}{\sqrt{Dg\cos\alpha}} \tag{12}$$

and where C_2 is a disturbance factor of an infinitesimal wave; $\tilde{u}_g$, $\tilde{h}_l$, $\widetilde{A}_l$, and $\widetilde{A}_g$ are the dimensionless gas velocity, the liquid filling height, the liquid and the gas core cross-section, respectively. All variables are normalized by the geometric constraints of a pipe. The transition criterion for the intermittent to annular flow regime is based on the result from Butterworth (1972), showing a wave of adequate height being swept around the wall forming the annular regime at an initial filling height of less than $\tilde{h}_l = 0.5$. This results, for the horizontal alignment of the tube, in a constant value of $X = 1.6$.

The criterion of Taitel and Dukler (1976) from the stratified smooth to wavy transition has limited or no relevance in the microscale two-phase flow. On the other hand, the transition regime from bubbly to intermittent flow is relevant and is based on their work on the equilibrium of the turbulent fluctuations of the flow and the buoyant forces of the gas bubbles yielding the following dimensionless criterion:

$$T^2 \geqslant \left[\frac{8\widetilde{A}_g}{\widetilde{S}_i\tilde{u}_l^2\left(\tilde{u}_l\widetilde{D}_l\right)^{-n}}\right] \tag{13}$$

with

$$T = \left[\frac{|(dP/dx)_{l,s}|}{(\rho_l - \rho_g)g\cos\alpha}\right]^{\frac{1}{2}} \tag{14}$$

where $\tilde{u}_l$, $\widetilde{A}_g$, $\widetilde{D}_l$, and $\widetilde{S}_i$ are the dimensionless liquid velocity, cross-section, hydraulic diameter and the surface area of the gas–liquid interface, respectively. All variables are normalized by the liquid filling level and the diameter of the pipe.

Even though the model proved to suitably predict phase transitions in macroscopic channels as shown in Taitel and Dukler (1976) for the flow maps of Mandhane et al. (1974) for a circular pipe of 25 mm diameter, the Taitel–Dukler model fails to predict flow transitions at smaller diameters, already below 5 mm as shown in the comparisons of Damiandides and Westwater (1988) and Coleman and Garimella (1999).

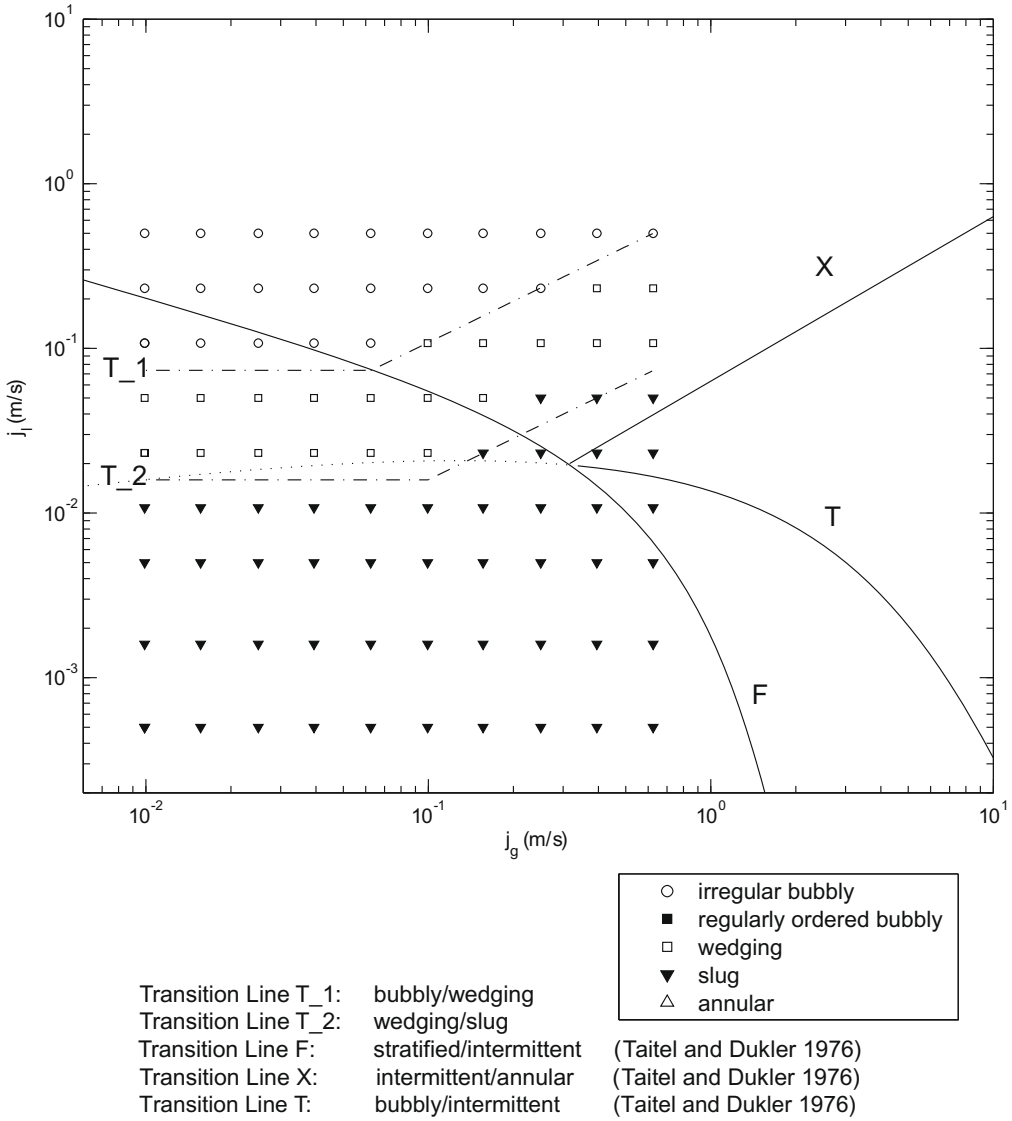

Fig. 7. Flow map comparison to the Taitel–Dukler model.

The comparison of the Taitel–Dukler model (Taitel and Dukler, 1976) with our parameter set 1, shown in Fig. 7, yields for the transition line F (phase transition between stratified and intermittent flow, based on the dimensionless criterion F) no agreement. Also, it has to be noted that the parameter set 1 did not depict any stratified flow; neither smooth, nor wavy. The applied criterion of an extended Kelvin–Helmholtz Theory does not satisfactorily explain wave growth in microfluidics.

On the other hand, the Taitel–Dukler-based transition line excluding the intermittent from the annular flow regime (transition line *X*, based on $X = 1.6$) shows a comparable slope as our experimentally obtained transitions from wedging to slug flow. This apparent coincidence still can bear an interesting piece of information about the validity of the model: Although the channel geometry causes a deviation, the basic momentum balance concept is still valid.

The transition line intermittent to dispersed bubbly flow (transition line T, based on the dimensionless criterion T) only superimposes our data when extrapolated to smaller superficial gas velocities matching the transition line plateaus. However, this superposition has to be regarded as purely coincidental, since neither gravity-based buoyancy forces nor turbulent fluctuations play a significant role in microfluidics underestimating the important effect of surface tension completely.

The concluding remark regarding the original Taitel–Dukler model is that the lack of inclusion of the surface tension effect in the model, causes it to lose its applicability in microfluidics below the critical Bond Number of $Bo \leqslant 3.368$.

3.4.4. Comparison to modified Taitel Dukler model

The work of Barnea et al. (1983) presents a modification for the Taitel–Dukler model for smaller pipe diameters verified for channels of diameters of 4 mm and larger. The incorporation of surface tension as a relevant force for the transition from stratified to intermittent flow yields the following criterion:

$$\tilde{h}_l \geqslant (1 - \pi/4) \tag{15}$$

Fig. 8 shows the comparison of this criterion (transition line F_modified) to the present parameter set 3. It was found that the modified transition line matches the transition of slug to annular flow, see Fig. 8. Even though the momentum balances of the Taitel–Dukler model are based on a circular cross-section, it appears that the incorporation of the surface tension better predicts phase transitions in sub-millimeter microchannels.

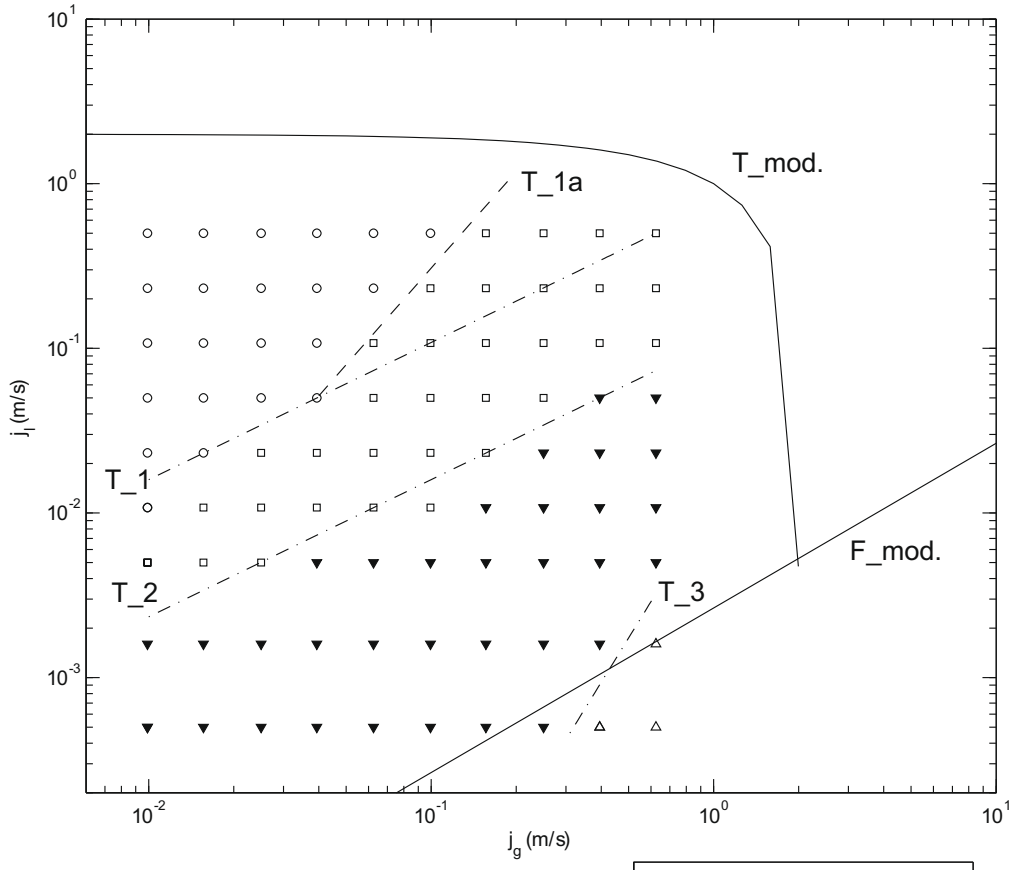

Fig. 8. Flow map comparison to the modified Taitel–Dukler model.

Another modification of the original Taitel–Dukler model has been presented by Brauner and Maron (1992) in order to achieve a better prediction of phase transitions in small diameters for the dispersed bubbly to stratified transition (transition line T_modified). The modifications implement a critical bubble size at which the surface tension is just preventing the formation of a continuous gas layer driven by buoyancy forces.

As discussed throughout the paper, below the critical Bond Number the reduced influence of gravity will not significantly affect the phase transition, as confirmed by the mismatch of the calculated transition line based on the modification of Barnea et al. (1983) to the parameter set 1 in Fig. 8.

The conclusions drawn from the comparison with the mechanistic model of Taitel and Dukler (1976) and its modifications from Barnea et al. (1983) and Brauner and Maron (1992) are that even though these models proved their validity for phase transitions in macroscopic channels and under the consideration of the modifications also in channels of diameters down to 4 mm, they are not reliable for two-phase flow below the critical Bond Number, due to the diminished influence of gravity, which does not any more prevail over surface tension.

4. Conclusion

The focus of this paper is the experimental construction of flow maps of adiabatic two-phase flow in rectangular microchannels with an aspect ratio of unity and the comparison of these maps with other published experimental results. The influence of surface tension and nozzle geometry on the phase transition was investigated by a parametric study involving two nozzle widths and a set of liquid mixtures. The fluid mixture, water and methanol, with CO_2 as the gas phase, was chosen due to its relevance in important microfluidic applications, specifically in microscale direct methanol fuel cells. This allowed also the examination of the influence of surface tension. The incorporated nozzle geometry facilitated a broad range of different flow regimes such as bubbly, regularly ordered bubbly, wedging, slug and annular flows, depending on influencing factors such as nozzle and channel geometries and fluid properties.

The study of different methanol mixtures yielded a relatively small influence on the flow transitions within our experimental measurement domain. However, by increasing the methanol content in our fluid mixture, the stabilization of capillary bubbles was shown at lower superficial gas velocities. In addition, the occurrence of regularly ordered bubbles can be attributed to the mixing of methanol.

The comparison between the different nozzle widths resulted in a relation between the nozzle width and the stabilization of bubbles. The nozzle width is therefore an important parameter for two-phase flow maps in microfluidics. Smaller nozzle geometries and fluids of smaller surface tension promote capillary gas bubbles at lower superficial gas and liquid velocities also increasing the likelihood for the occurrence of regularly ordered bubbly flow.

Comparing our data to published experimentally obtained flow maps, a general agreement of flow transitions compared to Cubaud and Ho (2004), Zhao and Bi (2001), Triplett et al. (1999) was observed where relevant. Interestingly, the extrapolation of the wedge/slug flow transition from Zhao and Triplett to lower superficial velocities corroborates our detected annular flow regime of pure methanol, in contrast to Cubaud and Ho (2004). The argument in Cubaud and Ho (2004) that the channel size does not have an influence on phase transitions is not corroborated by our results. In contrast, our measurements of lower superficial liquid velocities display a transition plateau. A further important result in the present flow maps is the extension of the experimental knowledge base to smaller superficial liquid velocities (by almost two orders of magnitude compared to Cubaud and Ho (2004)). In addition, we report as a new finding the occurrence of regularly ordered bubbles in combination with flow maps placing them as a transition regime between dispersed bubbly and wedging flow.

The Taitel–Dukler model did not prove to be an adequate means to predict phase transitions in microscopic two-phase flow below the critical Bond Number. Further, the modifications from Brauner and Maron (1992) failed to predict the transition between the bubbly and the intermittent flow regime. The only partial agreement was found for the Barnea et al. (1983) modification.

Acknowledgements

The authors also would like to acknowledge Magnus Fischer from the Laboratory of Thermodynamics in Emerging Technologies of ETH Zurich for useful discussions.

References

Agrawal, S.S., Gregory, G.A., Govier, G.W., 1973. Analysis of horizontal stratified 2 phase flow in pipes. Can. J. Chem. Eng. 51, 280–286.
Amon, C.H., Murthy, J., Yao, S.C., Narumanchi, S., Wu, C.F., Hsieh, C.C., 2001. MEMS-enabled thermal management of high-heat-flux devices EDIFICE: embedded droplet impingement for integrated cooling of electronics. Exp. Therm. Fluid Sci. 25, 231–242.
Baker, O., 1954. Simultaneous flow of oil and gas. Oil Gas J. 53, 185–195.
Barnea, D., Taitel, Y., 1993. A model for slug length distribution in gas–liquid slug flow. Int. J. Multiphase Flow 19, 829–838.
Barnea, D., Luninski, Y., Taitel, Y., 1983. Flow pattern in horizontal and vertical 2 phase flow in small diameter pipes. Can. J. Chem. Eng. 61, 617–620.
Brauner, N., Maron, D.M., 1992. Identification of the range of small diameters conduits, regarding 2-phase flow pattern transitions. Int. Commun. Heat Mass Transfer 19, 29–39.
Bretherton, F.P., 1961. The motion of long bubbles in tubes. J. Fluid Mech. 10, 166–188.
Butterworth, D., 1972. A Visual Study of Mechanisms in Horizontal, Air-water Flow. AERE Report M2556; Harwell, England.
Choban, E.R., Markoski, L.J., Wieckowski, A., Kenis, P.J.A., 2004. Microfluidic fuel cell based on laminar flow. J. Power Sources 128, 54–60.
Coleman, J.W., Garimella, S., 1999. Characterization of two-phase flow patterns in small diameter round and rectangular tubes. Int. J. Heat Mass Transfer 42, 2869–2881.
Cubaud, T., Ho, C.M., 2004. Transport of bubbles in square microchannels. Phys. Fluids 16, 4575–4585.
Cubaud, T., Tatineni, M., Zhong, X.L., Ho, C.M., 2005. Bubble dispenser in microfluidic devices. Phys. Rev. E 72 (3).
Damiandides, C., Westwater, J.W., 1988.Two-phase flow patterns in a compact heat exchanger and in small tubes. In: Second UK National Conference On Heat Transfer, Glasgow, Scotland, pp. 1257–1268.
Darmana, D., Deen, N.G., Kuipers, J.A.M., 2005. Detailed modeling of hydrodynamics, mass transfer and chemical reactions in a bubble column using a discrete bubble model. Chem. Eng. Sci. 60, 3383–3404.
Dollet, B., van Hoeve, W., Raven, J.P., Marmottant, P., Versluis, M., 2008. Role of the channel geometry on the bubble pinch-off in flow-focusing devices. Phys. Rev. Lett. 100 (3).
Dudukovic, M.P., Larachi, F., Mills, P.L., 1999. Multiphase reactors – revisited. Chem. Eng. Sci. 54, 1975–1995.
Escher, W., Michel, M., Poulikakos, D., 2009. Efficiency of optimized bifurcating tree-like and parallel microchannel networks in the cooling of electronics. Int. J. Heat Mass Transfer 52, 1421–1430.
Fries, D.M., Waelchli, S., von Rohr, P.R., 2008. Gas–liquid two-phase flow in meandering microchannels. Chem. Eng. J. 135S, S37–S45.
Ganan-Calvo, A.M., Gordillo, J.M., 2001. Perfectly monodisperse microbubbling by capillary flow focusing. Phys. Rev. Lett. 87, 274501. 1–4.
Gordillo, J.M., Cheng, Z.D., Ganan-Calvo, A.M., Marquez, M., Weitz, D.A., 2004. A new device for the generation of microbubbles. Phys. Fluids 16, 2828–2834.
Gunther, A., Jensen, K.F., 2006. Multiphase microfluidics: from flow characteristics to chemical and materials synthesis. Lab on a Chip 6, 1487–1503.
Hassan, I., Vaillancourt, M., Pehlivan, K., 2005. Two-phase flow regime transitions in microchannels: a comparative experimental study. Microscale Thermophys. Eng. 9, 165–182.
Hotz, N., Lee, M.T., Grigoropoulos, C.P., Senn, S.M., Poulikakos, D., 2006a. Exergetic analysis of fuel cell micropowerplants fed by methanol. Int. J. Heat Mass Transfer 49, 2397–2411.
Hotz, N., Senn, S.M., Poulikakos, D., 2006b. Energy analysis of a solid oxide fuel cell micro power plant. J. Power Sources 158, 333–347.
Joanicot, M., Ajdari, A., 2005. Applied physics – droplet control for microfluidics. Science 309, 887–888.
Kattan, N., Thome, J.R., Favrat, D., 1998. Flow boiling in horizontal tubes. Part 3 – development of a new heat transfer model based on flow pattern. J. Heat Transfer Trans. ASME 120, 156–165.

Kew, P.A., Cornwell, K., 1997. Correlations for the prediction of boiling heat transfer in small-diameter channels. Appl. Therm. Eng. 17, 705–715.
Kobayashi, J., Mori, Y., Okamoto, K., Akiyama, R., Ueno, M., Kitamori, T., Kobayashi, S., 2004. A microfluidic device for conducting gas–liquid–solid hydrogenation reactions. Science 304, 1305–1308.
Kreutzer, M.T., Kapteijn, F., Moulijn, J.A., Heiszwolf, J.J., 2005. Multiphase monolith reactors: chemical reaction engineering of segmented flow in microchannels. Chem. Eng. Sci. 60, 5895–5916.
Lockhart, R.W., Martinelli, R.C., 1949. Proposed correlation of data for isothermal 2-phase, 2-component flow in pipes. Chem. Eng. Prog. 45, 39–48.
Lu, G.Q., Wang, C.Y., Yen, T.J., Zhang, X., 2004. Development and characterization of a silicon-based micro direct methanol fuel cell. Electrochim. Acta 49, 821–828.
Madou, M.J., 2002. Fundamentals of Microfabrication: The Science of Miniaturization. CRC Press, Boca Raton, FL.
Mandhane, J.M., Gregory, G.A., Aziz, K., 1974. A flow pattern map for gas–liquid flow in horizontal pipes. Int. J. Multiphase Flow 1, 537–553.
Millies, M., Mewes, D., 1999. Interfacial area density in bubbly flow. Chem. Eng. Process. 38, 307–319.
Romera-Guereca, G., Choi, T.Y., Poulikakos, D., 2008. Explosive vaporization and microbubble oscillations on submicron width thin film strip heaters. Int. J. Heat Mass Transfer 51, 4427–4438.
Rosengarten, G., Mutzenich, S., Kalantar-zadeh, K., 2006. Integrated micro thermoelectric cooler for microfluidic channels. Exp. Therm. Fluid Sci. 30, 821–828.
Senn, S.M., Poulikakos, D., 2004. Laminar mixing, heat transfer and pressure drop in tree-like microchannel nets and their application for thermal management in polymer electrolyte fuel cells. J. Power Sources 130, 178–191.
Senn, S.M., Poulikakos, D., 2005. Multiphase transport phenomena in the diffusion zone of a PEM fuel cell. J. Heat Transfer Trans. ASME 127, 1245–1259.
Taitel, Y., Dukler, A.E., 1976. Model for predicting flow regime transitions in horizontal and near horizontal gas–liquid flow. AIChE J. 22, 47–55.
Taylor, G.I., 1960. Deposition of a viscous fluid on the wall of a tube. J. Fluid Mech. 10, 161–165.
Thonon, B., Vidil, R., Marvillet, C., 1995. Recent research and developments in plate heat-exchangers. J. Enhanced Heat Transfer 2, 149–155.
Triplett, K.A., Ghiaasiaan, S.M., Abdel-Khalik, S.I., Sadowski, D.L., 1999. Gas–liquid two-phase flow in microchannels. Part I: two-phase flow patterns. Int. J. Multiphase Flow 25, 377–394.
Vanhouten, R.T., Pol, L.W.H., Lettinga, G., 1994. Biological sulfate reduction using gas-lift reactors fed with hydrogen and carbon-dioxide as energy and carbon source. Biotechnol. Bioeng. 44, 586–594.
Waelchli, S., von Rohr, P.R., 2006. Two-phase flow characteristics in gas–liquid microreactors. Int. J. Multiphase Flow 32, 791–806.
Webb, R.L., 2004. Odyssey of the enhanced boiling surface. J. Heat Transfer Trans. ASME 126, 1051–1059.
Zhao, T.S., Bi, Q.C., 2001. Co-current air–water two-phase flow patterns in vertical triangular microchannels. Int. J. Multiphase Flow 27, 765–782.